69th International Astronautical Congress, Bremen, Germany.

IAC-18.C1.4.3x42523

Closed-Chain Forward Dynamics Modeling of a Four-Body Folding Spacecraft Structure

JoAnna Fulton[a,*] and Hanspeter Schaub[b]

[a] *Graduate Research Assistant, Department of Aerospace Engineering Sciences, University of Colorado, 431 UCB, Colorado Center for Astrodynamics Research, Boulder, CO 80309-0431.*, joanna.fulton@colorado.edu

* Corresponding Author

[b] *Glenn L. Murphy Endowed Chair, Associate Chair of Graduate Affairs, Department of Aerospace Engineering Sciences, University of Colorado, 431 UCB, Colorado Center for Astrodynamics Research, Boulder, CO 80309-0431.*, hanspeter.schaub@colorado.edu

Abstract

This paper analyzes the dynamic behavior and develops the equations of motion of an origami folded spacecraft structure. The dynamics model is derived using the augmented approach for closed-chain forward dynamics. This is a multi-body approach developed in the literature for complex robotic manipulator systems. In this paper, we demonstrate the applicability of this approach to folded deployable spacecraft structures. This approach is desirable due to the computational efficiency of the algorithm and the ability to implement multiple types of complex internal hinge behavior without reformulation of the dynamics algorithm.

1. Nomenclature

2. Acronyms/Abbreviations

3. Introduction

The size and weight constraints of launch vehicles have inspired the development of innovated deployable spacecraft structures technologies.[1] An emerging area in this field takes inspiration from origami folding techniques to stow flat structures with large area relative to the spacecraft bus size, such as solar arrays,[2] star occulters,[3] and antenna.[4] A central challenge for this concept is the deployment dynamics and deployment actuation of the folded structure and spacecraft system. These concepts are often studied through expensive physical testing and prototyping or time costly finite element modeling. This paper considers modeling the system dynamics using multi-body techniques with potential energy at the fold hinges to actuate the deployment.

This paper analyzes the dynamic behavior and develops the equations of motion of an origami folded spacecraft structure. The dynamics model is derived using the augmented approach for closed-chain forward dynamics. This is a multi-body approach developed in the literature for complex robotic manipulator systems.[5] In this paper, the applicability of this approach is demonstrated to folded deployable spacecraft structures. This approach is desirable due to the computational efficiency of the algorithm and the ability to implement multiple types of complex internal hinge behavior without reformulation of the dynamics algorithm. Investigations following the Lagrangian approach provide initial understand of the problem,[6] but are insufficient for scaling to multiple closed chain systems. Additionally, Kane's method[7] is found to be insufficient in comparison to the framework provided by the spatial operator based model here. The advantageous partial velocities defined by Kane's method are also represented in the spatial operator models, however maintaining the full spatial operator model enables further algorithm development. Therefore, the model structure of the spatial operator format is viewed by some as a refinement of Kane's equations.[5]

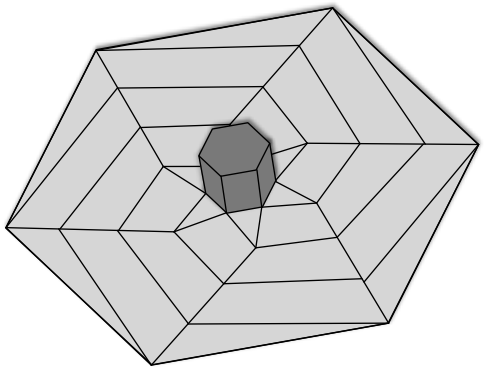

Fig. 1: Example concept: A spacecraft hub with a radially folding deployable structure.

Origami fold patterns with repeating structure, such as the Miura-Ori[8] and Scheel patterns,[9] are considered. These patterns share the common property of having no

more than four panels meeting at each vertex. Therefore, the subsystem case of a four-panel set is analyzed in detail as a starting point. A generic set of four panels folding at a vertex can be modeled as an undirected multiply connected graph or as a directed acyclic graph with similar qualities to a four bar mechanism. These two modeling options and their consequences are explored and discussed. The closed four-body chain is approached as two two-body arms subject to a system loop constraint and an algorithm to derive the generic equations of motion is developed. Error control methods on the loop constraint are implemented and discussed. The scalability of the algorithm to multiple-loop systems, as would be seen in a repeating origami pattern, is evaluated. Modeling the hinge actuation behavior is studied in detail.

Self-actuated deployable space structures are structures that stow internal strain or potential energy within the structural components when in the stowed configuration, that actuate the deployment when released, and that typically have no stored energy in the deployed configuration.[10] A simple example of this is a torsion spring actuating a single axis rotation to deploy a solar panel. High strain (large deformation) composites are an emerging technology that can provide self actuation at low mass and have diverse application.[11,12] Implementing high strain composite hinges in the joints of folded deployable structures eliminates the complexity and mass of a motorized external actuation structure while adding rigidity across joints. However, such hinges are flexible in multiple degrees of freedom and therefore have complex force and moment behavior. A primary motivation for selecting the articulated body forward dynamics algorithm for this modeling case is the analysis advantages provided by the hinge motion representation. These models must accommodate complex internal hinge models with multiple degrees of freedom. Furthermore, the constraints and parameters of the hinge motion must be able to be updated in a modular fashion as the internal hinge models are currently under development. This requirement is met by implementing the motion constraints of the hinges through the hinge map matrix definition, $H^{\intercal}(k)$, and providing the internal hinge behavior through the hinge force, $T(k)$.

4. Graph Theory and Folded Structures

4.1 Overview of Theory

A system of hinge-connected rigid bodies can be represented using graph theory by treating the rigid bodies as nodes and the hinges or fold lines as edges. This representation will aid in breaking down the complex system into a form that can be efficiently analyzed. The manner in which the system of nodes is connected determines the classification of the system. For a given graph, the node from which an edge leads from is designated the parent node, and the node at the destination of that edge is referred to as the child node. A parent node can have multiple child nodes, and if these nodes do not share edges within the graph, the graph is referred to as a tree topology. The basis of the dynamics algorithm discussed here is written to recursively solve for a serial chain of bodies, following the branch of a tree. At initial consideration, the closed-loop patterns of a folded spacecraft structure is a multiply connected digraph where multiple child nodes span from a parent node and are interconnected, and there exist paths in the graph that lead back to a given node. Then the first step in modeling a folded spacecraft structure is to identify edges of the system to "cut" such that the bodies are segmented into a tree topology. These cut edges must then be constrained to enforce the desired topology. The graph showing how these systems are broken down is referred to as a digraph.

4.2 Kinematic Chains of Planar Origami Patterns

The development and analysis of origami-inspired fold patterns appropriate for use in spacecraft structures is an active area of interest. A select number of patterns have received more study due to the clear applicability to spacecraft needs. The Miura-ori pattern, illustrated in Figure 2, is a highly efficient folding scheme with one theoretical degree of freedom that deploys linearly in a two direction, planar fashion and that is thoroughly studied in literature. Similarly, the Scheel pattern illustrated in Figure 3 is a radially wrapped pattern that is commonly studied for spacecraft structure applications.

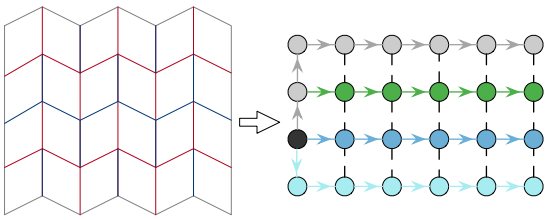

Fig. 2: Linearly configured Miura-ori folding pattern and example system digraph with cut edges.

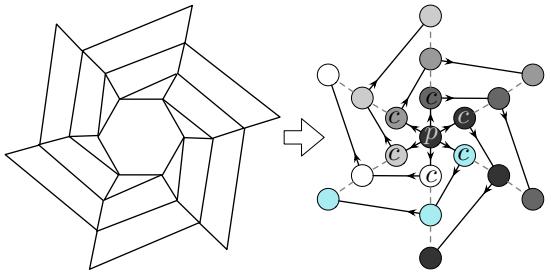

Fig. 3: Radially configured Scheel folding pattern and example digraph with cut edges.

Figures 2 and 3 also display example digraph patterns for their corresponding origami pattern. The patterns are

segmented such that a single root parent node spawns the serial chains of the origami pattern in a manner that itself displays a repeatable and expandable pattern. These serial chains are then constrained to each other at each adjacent node of their chains.

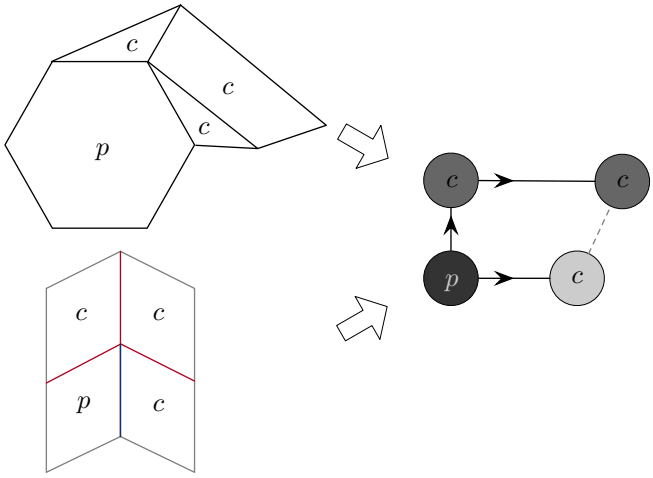

Fig. 4: Subgraph of 4 body closed-chain structure.

In both of these prominent patterns, and in many more not mentioned here, the complex systems of interconnected bodies are entirely comprised of four-body subgraphs, as illustrated in Figure 4. Additionally, the four-body system is the simplest system that embodies the challenges presented by closed-chain systems, where one cut-edge constraint is included. Therefore, the remainder of this analysis uses the four-body case to illustrate the approach. Additionally, the four-body subgraph is reminiscent of the classic four bar mechanism, although in this problem, the joint kinematics remain free in multiple degrees of freedom, where the four bar mechanism is typically constrained to one rotation per joint. However, further constraining the four-body model to mimic the four-bar mechanism provides a simple point of verification if needed.

5. Dynamics Theory

The dynamics algorithm applied here is derived from the $\mathcal{O}(\mathcal{N})$ Articulated-Body Forward Dynamics (ABFD) algorithm developed independently by Featherstone[13] and Rodriguez,[14] and detailed in a unified manner by Jain.[15] The algorithm is developed to be appropriate for any multi-body robotic system that is treated as a network of serial-chain rigid bodies. The full derivation of the algorithm can be reviewed in the literature, but key formulations are repeated here to provide context to the derivations developed here for spacecraft and deployable structure systems. In the articulated-body model, each of the rigid bodies down-chain of the current body being considered are treated as completely free with zero hinge force. Under this assumption, the articulated body inertia is calculated to represent those free bodies and a correction term is included to compensate for this assumption. This approach is in contrast to the composite body model, which treats the connected rigid bodies as fixed relative to each other, and uses a similar composite body inertia and correction term to derive the hinge force. However, the articulated body model is more appropriate for the forward dynamics problem.

5.1 Spatial Vectors

The ABFD algorithm is structured using spatial vectors for computational and mathematical efficiency. Spatial vector algebra uses six dimensional representations of rigid body properties to capture both the rotational and linear components in a single expression. For example, a rigid body's orientation and position, referred to as the spatial coordinates of frame $\mathcal{G}$ with respect to frame $\mathcal{F}$ as

$$\boldsymbol{q}(\mathcal{F},\mathcal{G}) = \begin{bmatrix} \boldsymbol{\theta}(\mathcal{F},\mathcal{G}) \\ \boldsymbol{l}(\mathcal{F},\mathcal{G}) \end{bmatrix} \tag{1}$$

where $\boldsymbol{\theta}$ is a three coordinate representation of orientation and $\boldsymbol{l}$ is the position vector in 3D Euclidean space. In this application, the orientation is represented by the standard 3-2-1 Euler Angles.[16] Similarly, the spatial velocity is chosen as the angular rotation rate and the linear velocity of the body

$$\boldsymbol{\beta}(\mathcal{F},\mathcal{G}) = \begin{bmatrix} \boldsymbol{\omega}(\mathcal{F},\mathcal{G}) \\ \boldsymbol{v}(\mathcal{F},\mathcal{G}) \end{bmatrix} \tag{2}$$

Where the relative angular velocity is a non-integrable quasi-velocity, meaning it is not the time derivative of the spatial coordinates, and the notation $\boldsymbol{\omega}(\mathcal{F},\mathcal{G})$ denotes the angular velocity of frame $\mathcal{G}$ with respect to frame $\mathcal{F}$. The spatial orientations and spatial angular velocities are then related to each other using a linear transformation. For 3-2-1 Euler angles, this transformation is[16]

$$\dot{\boldsymbol{\theta}} = \frac{1}{c\theta_2} \begin{bmatrix} 0 & s\theta_3 & c\theta_3 \\ 0 & c\theta_2 c\theta_3 & -c\theta_2 s\theta_3 \\ c\theta_2 & s\theta_2 s\theta_3 & s\theta_2 c\theta_3 \end{bmatrix} \boldsymbol{\omega} = [B]^{\omega}\boldsymbol{\omega} \tag{3}$$

where s and c are abbreviations for $\sin$ and $\cos$ respectively. Then the full spatial transformation is

$$\dot{\boldsymbol{q}} = [B]\boldsymbol{\omega} = \begin{bmatrix} [B]^{\omega} & 0_3 \\ 0_3 & I_3 \end{bmatrix} \boldsymbol{\omega} \tag{4}$$

5.1.1 Spatial Rigid Body Transformation

A key spatial vector operation to develop is the rigid body transformation between frames. For a frame that is both translating and rotating with respect to a reference frame, the 6×6 transformation that transforms a vector expressed in the $\mathcal{G}$ frame to one expressed in the $\mathcal{F}$ frame is

$${}^{\mathcal{F}}\boldsymbol{q} = \phi(\mathcal{F},\mathcal{G})^{\mathcal{G}}\boldsymbol{q} \tag{5}$$

where

$$\phi(\mathcal{F},\mathcal{G}) = \begin{bmatrix} I_3 & [{}^{\mathcal{F}}\tilde{\boldsymbol{l}}(\mathcal{F},\mathcal{G})] \\ 0_3 & I_3 \end{bmatrix} \begin{bmatrix} [\mathcal{F}\mathcal{G}] & 0_3 \\ 0_3 & [\mathcal{F}\mathcal{G}] \end{bmatrix} \tag{6}$$

where the 3×3 direction cosine matrix between frames $\mathcal{F}$ and $\mathcal{G}$ is represented by $[\mathcal{F}\mathcal{G}]$, I_3 is the 3×3 identity matrix, 0_3 is a 3×3 zero matrix, and the tilde operator is the cross product matrix operation for a 3 vector, defined as

$$[\tilde{\boldsymbol{l}}] = \begin{bmatrix} 0 & -l_3 & l_2 \\ l_3 & 0 & -l_1 \\ -l_2 & l_1 & 0 \end{bmatrix} \tag{7}$$

5.1.2 Spatial Rigid Body Transformation Derivative

The time derivative of the transposed spatial transformation is needed throughout the dynamics development to follow. Following Equation 6 and the matrix property $[\tilde{\boldsymbol{l}}]^{\intercal} = -[\tilde{\boldsymbol{l}}]$,

$$\phi^{\intercal}(\mathcal{F},\mathcal{G}) = \begin{bmatrix} [\mathcal{G}\mathcal{F}] & 0_3 \\ 0_3 & [\mathcal{G}\mathcal{F}] \end{bmatrix} \begin{bmatrix} I_3 & 0_3 \\ -[{}^{\mathcal{F}}\tilde{\boldsymbol{l}}(\mathcal{F},\mathcal{G})] & I_3 \end{bmatrix} \tag{8}$$

Using the chain rules

$$\begin{aligned} \frac{\mathrm{d}}{\mathrm{d}t}\phi^{\intercal}(\mathcal{F},\mathcal{G}) = & \\ & \frac{\mathrm{d}}{\mathrm{d}t}\begin{bmatrix} [\mathcal{G}\mathcal{F}] & 0_3 \\ 0_3 & [\mathcal{G}\mathcal{F}] \end{bmatrix} \begin{bmatrix} I_3 & 0_3 \\ -[{}^{\mathcal{F}}\tilde{\boldsymbol{l}}(\mathcal{F},\mathcal{G})] & I_3 \end{bmatrix} \\ & + \begin{bmatrix} [\mathcal{G}\mathcal{F}] & 0_3 \\ 0_3 & [\mathcal{G}\mathcal{F}] \end{bmatrix} \frac{\mathrm{d}}{\mathrm{d}t}\begin{bmatrix} I_3 & 0_3 \\ -[{}^{\mathcal{F}}\tilde{\boldsymbol{l}}(\mathcal{F},\mathcal{G})] & I_3 \end{bmatrix} \end{aligned} \tag{9}$$

The time derivative of the direction cosine matrix is known[16] to be

$$\frac{\mathrm{d}}{\mathrm{d}t}[\mathcal{G}\mathcal{F}] = -[\tilde{\boldsymbol{\omega}}(\mathcal{F},\mathcal{G})][\mathcal{G}\mathcal{F}] \tag{10}$$

and the derivative of the position vector expressed in frame $\mathcal{F}$ is denoted as $\boldsymbol{v}_{\mathcal{F}}(\mathcal{F},\mathcal{G})$, then

$$\begin{aligned} \frac{\mathrm{d}}{\mathrm{d}t}\phi^{\intercal}(\mathcal{F},\mathcal{G}) = & \begin{bmatrix} -[\tilde{\boldsymbol{\omega}}(\mathcal{F},\mathcal{G})] & 0_3 \\ 0_3 & -[\tilde{\boldsymbol{\omega}}(\mathcal{F},\mathcal{G})] \end{bmatrix} \phi^{\intercal}(\mathcal{F},\mathcal{G}) \\ & + \begin{bmatrix} 0_3 & 0_3 \\ -[\tilde{\boldsymbol{v}}_{\mathcal{F}}(\mathcal{F},\mathcal{G})] & 0_3 \end{bmatrix} \phi^{\intercal}(\mathcal{F},\mathcal{G}) \end{aligned} \tag{11}$$

Simplifying,

$$\frac{\mathrm{d}}{\mathrm{d}t}\phi^{\intercal}(\mathcal{F},\mathcal{G}) = -\begin{bmatrix} [\tilde{\boldsymbol{\omega}}(\mathcal{F},\mathcal{G})] & 0_3 \\ [\tilde{\boldsymbol{v}}_{\mathcal{F}}(\mathcal{F},\mathcal{G})] & [\tilde{\boldsymbol{\omega}}(\mathcal{F},\mathcal{G})] \end{bmatrix} \phi^{\intercal}(\mathcal{F},\mathcal{G}) \tag{12}$$

Defining a spatial vectrix operator as

$$\tilde{\boldsymbol{V}}_{\mathcal{F}}(\mathcal{F},\mathcal{G}) = \begin{bmatrix} [\tilde{\boldsymbol{\omega}}(\mathcal{F},\mathcal{G})] & 0_3 \\ [\tilde{\boldsymbol{v}}_{\mathcal{F}}(\mathcal{F},\mathcal{G})] & [\tilde{\boldsymbol{\omega}}(\mathcal{F},\mathcal{G})] \end{bmatrix} \tag{13}$$

Then the spatial transformation derivative is expressed as

$$\frac{\mathrm{d}}{\mathrm{d}t}\phi^{\intercal}(\mathcal{F},\mathcal{G}) = -\tilde{\boldsymbol{V}}_{\mathcal{F}}(\mathcal{F},\mathcal{G})\phi^{\intercal}(\mathcal{F},\mathcal{G}) \tag{14}$$

Note the similarities of structure with Equation 10, however the inclusion of the position offset of the frames to the transformation definition leads to an additional term.

5.1.3 Derivatives of Spatial Vectors

Consider the spatial vector transformation of a spatial vector expressed in the $\mathcal{G}$ frame to the $\mathcal{F}$ frame

$${}^{\mathcal{G}}\boldsymbol{x} = \phi^{\intercal}(\mathcal{F},\mathcal{G}){}^{\mathcal{F}}\boldsymbol{x} \tag{15}$$

Differentiating this expression using the chain rule yields

$$\frac{\mathrm{d}}{\mathrm{d}t}{}^{\mathcal{G}}\boldsymbol{x} = \frac{\mathrm{d}}{\mathrm{d}t}\phi^{\intercal}(\mathcal{F},\mathcal{G}){}^{\mathcal{F}}\boldsymbol{x} + \phi^{\intercal}(\mathcal{F},\mathcal{G})\frac{\mathrm{d}}{\mathrm{d}t}{}^{\mathcal{F}}\boldsymbol{x} \tag{16}$$

Using Equation 14, this expression becomes

$$\frac{\mathrm{d}}{\mathrm{d}t}{}^{\mathcal{G}}\boldsymbol{x} = -\tilde{\boldsymbol{V}}_{\mathcal{F}}(\mathcal{F},\mathcal{G})\phi^{\intercal}(\mathcal{F},\mathcal{G}){}^{\mathcal{F}}\boldsymbol{x} + \phi^{\intercal}(\mathcal{F},\mathcal{G})\frac{\mathrm{d}}{\mathrm{d}t}{}^{\mathcal{F}}\boldsymbol{x} \tag{17}$$

Then considering the coordinate-free notation, the time derivative of a spatial vector with respect to a given frame can be related to the time derivative of that spatial vector with respect to another frame through the following expression

$$\frac{{}^{\mathcal{G}}\mathrm{d}}{\mathrm{d}t}\boldsymbol{x} = \frac{{}^{\mathcal{F}}\mathrm{d}}{\mathrm{d}t}\boldsymbol{x} - \tilde{\boldsymbol{V}}_{\mathcal{F}}(\mathcal{F},\mathcal{G})\boldsymbol{x} \tag{18}$$

This equation draws parallels with the Transport Theorem for vectors in 3D Euclidean space.

5.2 Serial-chain ABFD Framework

The ABFD framework outlined by Jain[5] provides the basis of the version implemented here, with a few key adaptations that are described here as needed. The generalized spatial coordinates are chosen as hinge coordinates at the k^{th} hinge, or the k^{th} rigid body's outboard hinge frame, $\mathcal{O}_k$, orientation and position with respect to the $k+1$ rigid body's inboard hinge frame, $\mathcal{O}_k^+$, as illustrated in Figure 5,

$$\boldsymbol{q}(k) = \begin{bmatrix} \boldsymbol{\theta}(\mathcal{O}_k^+, \mathcal{O}_k) \\ \boldsymbol{l}(\mathcal{O}_k^+, \mathcal{O}_k) \end{bmatrix} \tag{19}$$

and the generalized velocities are chosen as the hinge spatial velocities, taken as the time derivative with respect to the $k+1$ frame

$$\boldsymbol{\beta}(k) = \begin{bmatrix} \boldsymbol{\omega}(\mathcal{O}_k^+, \mathcal{O}_k) \\ \boldsymbol{v}(\mathcal{O}_k^+, \mathcal{O}_k) \end{bmatrix} \tag{20}$$

For a given set of rigid bodies, these are collected in the full coordinate and velocity sets

$$q = \begin{bmatrix} \boldsymbol{q}(1) \\ \dots \\ \boldsymbol{q}(k) \\ \dots \\ \boldsymbol{q}(n) \end{bmatrix} \qquad \beta = \begin{bmatrix} \boldsymbol{\beta}(1) \\ \dots \\ \boldsymbol{\beta}(k) \\ \dots \\ \boldsymbol{\beta}(n) \end{bmatrix} \tag{21}$$

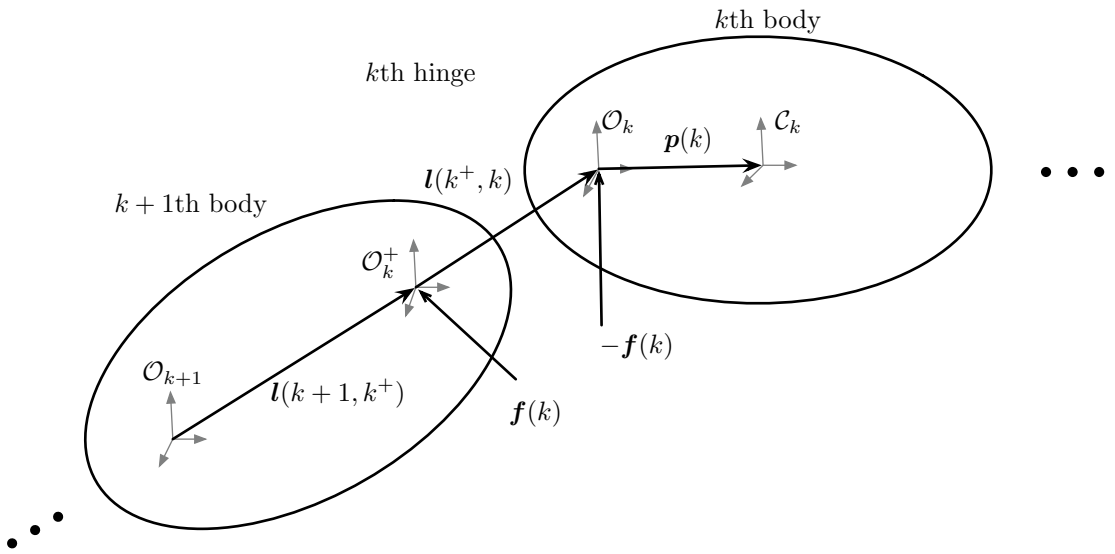

Fig. 5: Vector and frame notation between the $k+1$th and the kth body.

Where the tip of the chain is denoted as body 1 and the base body is denoted as body n. This leads to system equations of motion in the form

$$\mathcal{M}(q)\dot{\beta} + \mathcal{C}(q,\beta) = T \tag{22}$$

where $\mathcal{M}(q)$ is the full system mass matrix, $\mathcal{C}(q,\beta)$ contains the Coriolis contributions, and T is the vector of system generalized forces. The use of the quasi-velocities diverges from the assumptions implemented in Jain's text. In the forward dynamics problem, q, β and T are known quantities and the time derivative $\dot{\beta}$ is the desired quantity. Direct inversion of the mass matrix $\mathcal{M}$ is typically done for small order systems, but is a computationally expensive $\mathcal{O}(\mathcal{N}^3)$ matrix operation for an $\mathcal{N}$ size matrix. This becomes prohibitively slow for large DOF multibody systems. The computational efficiency of the ABFD algorithm is achieved by applying the Innovations Operator Factorization of the mass matrix $\mathcal{M}$ and deriving an explicit and analytical expression of the inverse, $\mathcal{M}^{-1}$. The details of this factorization are left to the literature. The dynamics are derived using body frame derivatives. The algorithm is set up in the following way. First, a recursive sweep that solves the velocities and Coriolis accelerations of the chain is run from the base body to the tip. Then, the articulated body inertias and corrections are solved for in a tip to base recursion. The final set is to do a base to tip recursion to solve for the body accelerations, yielding the system equations of motion.

5.2.1 Recursive Articulated Body Spatial Inertia

For a general rigid body where the hinge frame is not located at the center of mass, the spatial mass matrix about the hinge frame,$M(k)$, is

$$M(k) = \begin{bmatrix} J(k) & m(k)[\tilde{\boldsymbol{p}}(k)] \\ -m(k)[\tilde{\boldsymbol{p}}(k)] & mI_3 \end{bmatrix} \tag{23}$$

where

$$J(k) = J(c) + m(k)[\tilde{\boldsymbol{p}}(k)][\tilde{\boldsymbol{p}}(k)]^\intercal \tag{24}$$

is the body inertia about point k, $m(k)$ is the mass of the body, and $\boldsymbol{p}(k)$ is the position vector from the hinge frame to the center of mass frame of the kth body, illustrated in Figure 5 and expressed in the kth frame. The articulated body spatial inertia, $P(k)$ is then calculated as

$$P(k) = \phi(k,k-1)P^+(k-1)\phi^\intercal(k,k-1) + M(k) \tag{25}$$

where $P^+(k-1)$ is the projection of the $k-1$ articulated body inertia across the hinge frames. The correction force of the kth body is then

$$\boldsymbol{\zeta}(k) = \phi(k,k-1)\boldsymbol{\zeta}^+(k-1) + P(k)\boldsymbol{a}(k) + \boldsymbol{b}(k) \tag{26}$$

where $\boldsymbol{\zeta}^+(k-1)$ is the projection of the $k-1$ correction force and $b(k)$ is the Gyroscopic term, defined as

$$\boldsymbol{b}(k) = \bar{\boldsymbol{V}}(k)M(k)\boldsymbol{V}(k) \tag{27}$$

and the spatial bar operator is related to the spatial tilde operator as $\bar{\boldsymbol{x}} = -\tilde{\boldsymbol{x}}^\intercal$.

5.2.2 Recursive Velocity Kinematics

The spatial velocity kinematics for the n serial-chain bodies can be calculated recursively given the hinge coordinates and hinge velocities, where the $(n+1)$ body represents the non-accelerating fixed inertial frame and the

recursion runs from the base, nth, body to the tip, body 1.

$$\boldsymbol{V}(k) = \phi^{\intercal}(k+1,k)\boldsymbol{V}(k+1) + H^{\intercal}(k)\boldsymbol{\beta}(k) \quad (28)$$

where the relative velocity between bodies is the spatial hinge velocity

$$\boldsymbol{\Delta v}(k) = H^{\intercal}(k)\boldsymbol{\beta}(k) = H^{\intercal}(k)\begin{bmatrix}\boldsymbol{\omega}(\mathcal{O}_k^+,\mathcal{O}_k)\\ \boldsymbol{v}(\mathcal{O}_k^+,\mathcal{O}_k)\end{bmatrix} \quad (29)$$

5.2.3 Recursive Acceleration Derivation

The spatial acceleration is derived from the spatial velocity using Equation 18

$$\boldsymbol{\alpha}(k) = \frac{^{k}\mathrm{d}}{\mathrm{d}t}\boldsymbol{V}(k) = \frac{^{k+1}\mathrm{d}}{\mathrm{d}t}\boldsymbol{V}(k) - \tilde{\boldsymbol{\Delta v}}(k+1,k)\boldsymbol{V}(k) \quad (30)$$

For a rigid body, $\boldsymbol{\omega}(\mathcal{O}_k^+,\mathcal{O}_k) = \boldsymbol{\omega}(\mathcal{O}_{k+1},\mathcal{O}_k)$ and therefore $\boldsymbol{\omega}(k) = \boldsymbol{\omega}(k+1,k)$. The relative velocity

$$\begin{aligned}\boldsymbol{v}(k+1,k) = \frac{^{k+1}\mathrm{d}}{\mathrm{d}t}\boldsymbol{l}(k+1,k) = \\ \frac{^{k+1}\mathrm{d}}{\mathrm{d}t}\boldsymbol{l}(\mathcal{O}_{k+1},\mathcal{O}_{k^+}) + \frac{^{k+1}\mathrm{d}}{\mathrm{d}t}\boldsymbol{l}(\mathcal{O}_{k^+},\mathcal{O}_k) \\ = \boldsymbol{v}(\mathcal{O}_k^+,\mathcal{O}_k)\end{aligned} \quad (31)$$

and therefore $\boldsymbol{\Delta v}(k+1,k) = \boldsymbol{\Delta v}(k)$. The $k+1$ frame derivative of the spatial velocity is

$$\begin{aligned}\frac{^{k+1}\mathrm{d}}{\mathrm{d}t}\boldsymbol{V}(k) = \frac{^{k+1}\mathrm{d}}{\mathrm{d}t}\phi^{\intercal}(k+1,k)\boldsymbol{V}(k+1) \\ + \phi^{\intercal}(k+1,k)\frac{^{k+1}\mathrm{d}}{\mathrm{d}t}\boldsymbol{V}(k+1) \\ + \frac{^{k+1}\mathrm{d}}{\mathrm{d}t}H^{\intercal}(k)\boldsymbol{\beta}(k) + H^{\intercal}(k)\frac{^{k+1}\mathrm{d}}{\mathrm{d}t}\boldsymbol{\beta}(k)\end{aligned} \quad (32)$$

The hinge map matrix is assumed to be invariant for this case and therefore $\frac{^{k+1}\mathrm{d}}{\mathrm{d}t}H^{\intercal}(k)$ is zero. The spatial acceleration can then be expressed as

$$\begin{aligned}\boldsymbol{\alpha}(k) = \phi^{\intercal}(k+1,k)\boldsymbol{\alpha}(k+1) + H^{\intercal}(k)\dot{\boldsymbol{\beta}}(k) \\ + \frac{^{k+1}\mathrm{d}}{\mathrm{d}t}\phi^{\intercal}(k+1,k)\boldsymbol{V}(k+1) - \tilde{\boldsymbol{\Delta v}}(k+1,k)\boldsymbol{V}(k)\end{aligned} \quad (33)$$

Defining the Coriolis acceleration for the kth body as

$$\boldsymbol{a}(k) = \frac{^{k+1}\mathrm{d}}{\mathrm{d}t}\phi^{\intercal}(k+1,k)\boldsymbol{V}(k+1) - \tilde{\boldsymbol{\Delta v}}(k+1,k)\boldsymbol{V}(k) \quad (34)$$

the acceleration term is then

$$\boldsymbol{\alpha}(k) = \phi^{\intercal}(k+1,k)\boldsymbol{\alpha}(k+1) + H^{\intercal}(k)\dot{\boldsymbol{\beta}}(k) + \boldsymbol{a}(k) \quad (35)$$

and this expression also possesses a recursive structure. The Coriolis acceleration expression is then completed, where from Equation 14, the derivative of the spatial transformation matrix is

$$\frac{^{k+1}\mathrm{d}}{\mathrm{d}t}\phi^{\intercal}(k+1,k) = -\tilde{\boldsymbol{\Delta v}}(k+1,k)\phi^{\intercal}(k+1,k) \quad (36)$$

Then the Coriolis acceleration is

$$\begin{aligned}\boldsymbol{a}(k) = -\tilde{\boldsymbol{\Delta v}}(k+1,k)\phi^{\intercal}(k+1,k)\boldsymbol{V}(k+1) \\ - \tilde{\boldsymbol{\Delta v}}(k+1,k)\boldsymbol{V}(k)\end{aligned} \quad (37)$$

5.3 Capturing Complex Hinge Behavior

5.3.1 Hinge Mapping

The interaction of adjacent bodies in the chain are governed by the properties of the hinge connecting these bodies. The hinge map matrix, $H^{\intercal}(k)$, for a rigid body joint k defines the configuration dependence of the hinge behavior and maps the hinge velocities to the generalized spatial velocities of the body. Where $r_v(k)$ is the number of velocity degrees of freedom across the hinge, $H^{\intercal}(k) \in R^{6\times r_v(k)}$. For a free-floating rigid body in space, the hinge map matrix is a 6×6 identity matrix, I_6. Therefore, the spacecraft base-body is mapped to inertial space with I_6. This mapping introduces a simple and modular way to implement velocity constraints across the hinge of two adjacent bodies without reformulation of the dynamics algorithm. To maintain generality, the hinges of the four panel system are each given full six degrees of freedom.

5.3.2 Internal Hinge Forces

The spatial force acting at hinge k due to the interaction with body $k+1$ is denoted $f(k)$, where $f(k)$ acts at the O_k hinge frame and an equal but opposite force $-f(k)$ acts at the O_k^+ frame on the $k+1$ body. Then the generalized force on the k^{th} hinge, $T(k)$, is the projection of the spatial force through the hinge degrees of freedom, defined as

$$T(k) = H(k)f(K) \quad (38)$$

This force can be defined by the components in the hinge system. Examples of simple uncontrolled hinge forces are linear and torsion springs. Additionally, actuation components such as those used in robot arms could be installed at the hinge to control the multi-body motion. These type of actuators are not relevant to deployable origami structure research, however, due to the pursuit of a free, self-actuated deployment system. The hinges are therefore expected to contain strain or potential energy driven forces that are a function of the general coordinates.

5.4 Conserved Principles for Multi-body Systems

The conservation of energy and the conservation of momentum provide robust verification of the approach applied here. These principles are defined for spatial notation as follows.

5.4.1 Energy

The energy of a body is invariant across all points on the body, therefore for a given body k, the kinetic energy of the body about it's hinge frame is the same as the kinetic energy about it's center of mass. In spatial coordinates, this can be expressed as

$$KE(k) = \frac{1}{2}V(k)M(k)V(k) \tag{39}$$

And for a hinge with simple springs, the potential energy is

$$PE(k) = \frac{1}{2}q(k)K(k)q(k) \tag{40}$$

Where $K(k)$ is the stiffness matrix for the kth hinge, assuming a liner spring force as a function of the hinge general coordinates. The energy calculated at a each body is invariant to the frame that it is calculated at, so the total system energy can be calculated, independent of frame as

$$E = \sum_{k=1}^{n} KE(k) + PE(k) \tag{41}$$

5.4.2 Angular Momentum

The magnitude of the angular momentum of a single body about the body center of mass is conserved, where the angular momentum can be written in spatial coordinates as

$$h(c) = M(c)V(c) = \phi(C,k)h(k) = \phi(C,k)M(k)V(k) \tag{42}$$

For a system of rigid bodies, the angular momentum of each body expressed in the inertial frame is conserved. Therefore, the angular momentum of the system is calculated in the inertial frame as

$$h = \sum_{k=1}^{n} h_I(k) = \sum_{k=1}^{n} \phi(I,k)M(k)V(k) \tag{43}$$

Where the $n+1$ body referenced in the serial chain is the inertial reference frame, the rigid body transformation from a given hinge frame k to the inertial frame can be solved recursively

$$\phi(n+1,k) = \prod_{i=k}^{n} \phi(i+1,i) \tag{44}$$

5.5 Closed-Chain Forward Dynamics

As discussed in Section 4., capturing the closed-chain behavior is achieved by cutting an edge of a closed-chain system and treating each leg of the cut as an open serial chain, emulating a tree topology. Then the cut edges are treated as motion constraints imposed on the free dynamics of the tree. There are several approaches to enforcing the closure constraints. The augmented approach compensates for the cut edge by including a correction, resulting in additional motion constraint equations and a non-minimal coordinate set. This approach requires the use of differential-algebraic equation integrators and faces issues with error drift that must be compensated for with error control techniques. The direct approach uses matrix solvers and absolute coordinates, resulting in a much larger system and greater computational complexity. This approach also shares similar issues as the augmented approach, and therefore is not considered, as the augmented approach is more desirable for this application. A new technique that provides a minimal coordinate set is the constraint embedding approach. In this approach, the non-tree digraph is transformed into a tree topology by aggregating the closed-chain structures of the topology into a representative node. This is suitable for systems with a clear tree-like structure behind the closed-chain elements. The folded structures of interest contain multiply dependent systems of closed loops, as demonstrated in Figures 2 and 3, and therefore this approach is not well suited to the problems of interest and is not currently considered. Therefore, the augmented approach is selected and developed for the four body closed-chain example structure.

5.5.1 Augmented Approach to Closed Chain Structures

Implementing a correction term to account for the motion constraints is captured in the system equations of motion by introducing the Lagrange Multipliers,[5] denoted as λ, to represent the constraint forces. Additionally, a new set of equations must be considered to include the constraint expression. Defining a holonomic constraint expression as

$$\boldsymbol{d}(q,t) = \mathbf{0} \tag{45}$$

Taking the derivative, the holonomic constraint can be expressed in terms of a non-integrable set of velocity coordinates as

$$\dot{\boldsymbol{d}}(\beta,q,t) = \mathcal{G}_c(q,t)[B(q)]\dot{\beta} - U(t) = \mathbf{0} \tag{46}$$

where $[B]$ is defined in Equation 4, the term U is defined as

$$U(t) = -\frac{\partial}{\partial t}\boldsymbol{d}(q,t) \tag{47}$$

and

$$\mathcal{G}_c(q,t) = \nabla_q \boldsymbol{d}(q,t) \tag{48}$$

Then, defining the constraint force as $\mathcal{G}_c^{\intercal}(q,t)\lambda$, the full equations of motion are written as

$$\mathcal{M}(q)\dot{\beta} + \mathcal{C}(q,\beta) - \mathcal{G}_c^{\intercal}(q,t)\lambda = T \tag{49}$$

$$\mathcal{G}_c(q,t)[B(q)]\dot{\beta} = U(t) \tag{50}$$

The generalized acceleration is then redefined as

$$\dot{\beta} = \dot{\beta}_f + \dot{\beta}_c \tag{51}$$

where $\dot{\beta}_f$ are the free unconstrained accelerations and $\dot{\beta}_c$ are the correction accelerations. The correction acceleration is derived from the constraint expression, and is expressed in terms of spatial operators as

$$\dot{\beta}_c = [I - H\phi K]D^{-1}H\phi\mathcal{B}Q^{\intercal}\lambda \tag{52}$$

where H is the hinge map matrix, ϕ is the spatial transformation matrix, K is a spatial operator referred to in literature as the shifted Kalman gain operator, D is the articulated body hinge inertia, $\mathcal{B}$ is a node pick-off operator that identifies relevant nodes on the bodies of the system, Q is the constraint matrix, and λ is the Lagrange Multipliers. These are defined for loop constraints as

$$\lambda = -[Q\Lambda Q^{\intercal}]^{-1}\ddot{\boldsymbol{d}} \tag{53}$$

where Λ is the operation space compliance matrix $\Lambda = \mathcal{B}^{\intercal}\phi^{\intercal}H \intercal D^{-1}\phi H\mathcal{B}$. Differentiating the constraint expression,

$$\ddot{\boldsymbol{d}}(\beta, q, t) = \mathcal{G}_c(q,t)([B(q)]\ddot{\beta} + [\dot{B}(q)]\beta) - \dot{U}(t) \tag{54}$$

These equations establish the basis of the augmented approach for solving a system of closed-chain rigid bodies described using quasi-velocities as the generalized spatial velocities, where the literature has established this framework for using the time derivative of the spatial coordinates as the spatial velocities.

5.6 Closed-Chain Algorithm

An algorithm for solving the dynamics of a set of rigid bodies subject to a loop constraint is summarized in Table 1. This algorithm is applicable to systems beyond the four-body case of interest here, and can be extended to multiple closed-chain constraints within a system. The resulting equations of motion are subject to differential-algebraic equation integration to simulate the time history of the system.

Table 1: Closed-chain with loop constraint algorithm.

a. Define cut edges of digraph nodes
b. Solve for $\dot{\beta}_f$, $\dot{q}_f$ using ABFD for each tree branch
1. base to tip recursion for velocities, coriolis and gyroscopics
2. tip to base recursion for articulated inertias
3. base to tip recursion for hinge accelerations
c. compute $\ddot{\boldsymbol{d}}$, Λ, solve for Lagrange multipliers, λ
d. Compute Equation 52 for correcting accelerations
e. Compute Equation 51 for generalized accelerations

6. The Four-Body Structure Case

The closed-chain theory is now applied to the four-body structure case. Using the notation displayed in Figure 6, the cut edge is selected at the internal edge connecting

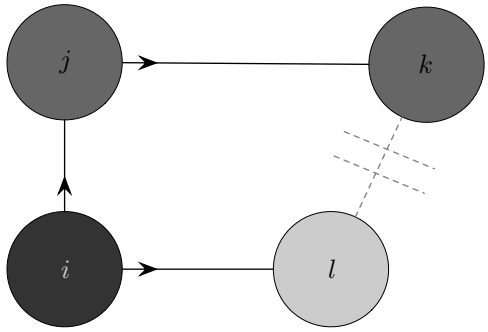

Fig. 6: Notation of 4 body closed-chain structure.

nodes k and l, where the root parent node is selected as node i. Due to the non-integrable spatial velocities, the closure constraint is better expressed as a non-holonomic constraint, expressed in the Pfaffian form as

$$\dot{\boldsymbol{d}}(\beta, t) = QV_n d - U = \begin{bmatrix} Q_l & -Q_k \end{bmatrix}\begin{bmatrix} V_l \\ V_k \end{bmatrix} - U = \mathbf{0} \tag{55}$$

where Q is the constraint matrix relating rigidly constrained velocity degrees of freedom between nodes l and k. A fully constrained node would have an identity matrix for the corresponding constraint matrix. Using the spatial velocity based expression in the Pfaffian form avoids the need for coordinate partials.

6.1 Loop Constraints and Error Control

By treating the closed-chain constraint as a correction to be applied to a free system, the problem becomes set up such that error in the correction becomes a greater concern. The correction error must be managed over time. It is suggested that this error be managed by introducing a stabilization term, such as the Baumgarte stabilization technique, to bound position and velocity errors.[17] Investigating this is left to future work.

7. Conclusions and Future Work

The challenges of developing a forward dynamics model of a self-actuated folded deployable spacecraft structure are outlined. Techniques developed for robotics applications are explored and found to be uniquely able to address the challenges of this problem. The articulated body forward dynamics algorithm is outlined as the basis for the approach, and derivations that generalize the ABFD algorithm to the spacecraft folded deployable structure scenario are provided. Approaches to the closed-chain constraint problem are outlined, and the augmented approach is developed for the four-body spacecraft structure. It is found that this approach provides significant value over the Lagrangian approach or Kane's equations. This is due to the computation gains of the recursive structure of the equations of motion and that the algorithm provides a framework for working with multiple rigid bodies. Future work will focus on developing algorithms for solv-

ing multiple closed-chain loops and integrating complex hinge force models.

8. Acknowledgments

The author acknowledges the NASA Space Technology Research Fellowship program and the Ann and H.J. Smead Department of Aerospace Engineering Sciences Smead Fellowship program for their generous support of this research.

REFERENCES

[1] Jeremy Banik. *Frontiers of Engineering: Reports on Leading-Edge Engineering from the 2015 Symposium*, chapter Realizing Large Structures in Space. the National Academies Press, 2015.

[2] Sungeun K. Jeon and Joseph N. Footdale. Scaling and design of a modular origami solar array. In *AIAA SciTech Spacecraft Structures Conference*, 2018.

[3] David Webb, Brian Hirsch, Vinh Bach, Jonathan Sauder, Case Bradford, and Mark Thomson. Starshade mechanical architecture and technology effort. In *3rd AIAA Spacecraft Structures Conference*, 2016.

[4] Daniel Kling, Sungeun Jeon, and Jeremy Banik. Novel folding methods for deterministic deployment of common space structures. In *3rd AIAA Spacecraft Structures Conference*, 2016.

[5] Abhinandan Jain. *Robot and Multibody Dynamics*. Springer Science+Business Media, LLC, 2011.

[6] JoAnna Fulton and Hanspeter Schaub. Dynamic modeling of folded deployable space structures with flexible hinges. In *2017 AAS/AIAA Astrodynamics Specialist Conference*, Stevenson, WA, 2017.

[7] Thomas R. Kane and David A. Levinson. *Dynamics: Theory and Applications*. McGraw-Hill, Inc., New York, 1985.

[8] Koryo Miura and Tomohiro Tachi. Synthesis of rigid-foldable cylindrical polyhedra. *Symmetry: Art and Science*, 2010.

[9] S.D. Guest and Sergio Pellegrino. Inextensional wrapping of flat membranes. In *Proceedings of the First International Seminar on Structural Morphology*, 1992.

[10] JoAnna Fulton, Sungeun Jeon, and Thomas W. Murphey. Flight qualification testing of a meter-class cubesat deployable boom. In *4th AIAA Spacecraft Structures Conference*, Kissimmee, FL, January 2017.

[11] Thomas W. Murphey and Sergio Pellegrino. A novel actuated composite tape-spring for deployable structures. In *45th AIAA/ASME/ASCE/AHS/ASC Structures, Structural Dynamics and Materials Conference*, 2004.

[12] Thomas W. Murphey, Michael E. Peterson, and Mikhail M. Grigoriev. Four point bending of thin unidirectional composite laminas. In *54th AIAA/ASME/ASCE/AHS/ASC Structures, Structural Dynamics, and Materials Conference*, Boston, Massachusetts, April 2013.

[13] Roy Featherstone. The calculation of robot dynamics using articulated-body inertias. *The International Journal of Robotics Research*, 2(1):13–30, Spring 1983.

[14] Guillermo Rodriguez. Recursive forward dynamics for multiple robot arms moving a common task object. *IEEE Transactions on Robotics and Automation*, 5(4):510–521, August 1989.

[15] Abhinandan Jain. Unified formulation of dynamics for serial rigid multibody sytems. *Journal of Guidance, Control, and Dynamics*, 14(3):531–542, May-June 1991.

[16] Hanspeter Schaub and John L. Junkins. *Analytical Mechanics of Space Systems*. American Institute of Aeronautics and Astronautics, Inc., Reston, Virginia, 20191-4344, 4th edition, 2018.

[17] Roy Featherstone. *Rigid Body Dynamics Algorithms*. Springer Science+Business Media, LLC, 2008.